Non-steady-state photoelectromotive force induced by a vibrating Ronchi grating: manifestation of a fractal structure

Nikolai Korneev, Ponciano Rodriguez-Montero,* and Svetlana Mansurova

National Institute for Astrophysics, Optics and Electronics, A.P. 51, Puebla 72000, Mexico
*Corresponding author: ponciano@inaoep.mx

We demonstrate that the non-steady-state photoelectromotive force induced by a vibrating Ronchi grating has a very complicated but deterministic dependence on the propagation distance. The characteristic minima of this dependence are found at fractional values of the Talbot distance, and their width is determined by the maximal transversal spatial frequency resolved by the system. This permits high accuracy in the determination of the Talbot distance.   © 2013 Optical Society of America

OCIS codes: 050.1950, 070.6760, 120.1088, 160.5140.

1. INTRODUCTION

The light intensity distribution after a grating illuminated by a plane wave is unexpectedly complicated. It was first observed by Talbot in the 19th century that the intensity distribution after a grating repeats itself exactly at even multiples of the propagation length z_0, known as the Talbot distance [1]. The theory of the effect was later given by Rayleigh [2,3]. In the paraxial approximation, the Talbot distance is given by $z_0 = d^2/\lambda$, where d is the period of the grating and λ is the illuminating wavelength. In 1996, Berry and Klein described the fractal structure of the Talbot effect [4]. For rational parts of the Talbot distance z_0, i.e., $z = z_0 q/p$ (with integers q and p), the image is composed of p copies of the initial distribution, shifted $1/p$ part of a period from each other. The field amplitudes from different copies are added with phase factors, and these factors are related to Gauss sums from number theory [4]. For Ronchi gratings stepwise distributions appear. For propagation lengths irrational with respect to the Talbot length, it was shown in [4] that the intensity distribution has fractal structure; i.e., similar shape is reproduced at all scales.

Physically, the fractal structure is limited by the finite spatial bandwidth. Factors such as the finite size of the grating and the breaking of the paraxial approximation contribute to the disappearance of fractals at a certain small scale. Fractals exist in longitudinal coordinates as well, in function of the distance from the grating [4].

An effort has been made to observe directly these phenomena in the optical domain. In particular, transverse and longitudinal patterns were measured in [4], and in [5] measurements of Talbot carpets were reported. Similar effects are observed in quantum mechanics as well [6,7].

We consider here the manifestation of the longitudinal fractal structure of the Talbot effect in the non-steady-state photoelectromotive force (photoEMF) induced by the light diffraction on a vibrating Ronchi grating. The photoEMF is a technique based on the properties of highly resistive photoconductors, which produce an electric current when they are illuminated with a moving (vibrating) pattern of light [8,9]. The photoEMF effect has been extensively used for the determination of photoconductor properties such as the photocarrier sign and diffusion length [10]. Applications to the detection of laser-generated ultrasound [11], correlation analysis [12,13], measurements of the coherence length [14], and for measuring the visibility of Fresnel diffraction patterns were demonstrated [15]. We show that, because of the special character of the detection process, the longitudinal fractal structure of the Talbot effect becomes very prominent here and the magnitude of the photoEMF current as a function of distance to the grating has a complicated deterministic multispike character, with a big number of narrow spikes, some of which are centered on positions that are simple fractions of the Talbot distance. The spike width is mainly determined by the numerical aperture of the grating; this width diminishes if the detector is placed closer to the grating.

The study of photoEMF induced by a vibrating Ronchi grating is not only interesting from a theoretical viewpoint. Geometries with Ronchi gratings are widely used for optical systems testing [3,16–19] and for several metrological applications [20–23]. We show that, from the positions of the minimal current in the photoEMF dependence on the propagation distance, the Talbot distance can be determined with high precision (of the order of 10^{-4} of the Talbot distance).

This paper is organized as follows. In Section 2 we briefly review the main features of the light field amplitude distribution generated by the diffraction on a Ronchi grating, illuminated by a plane wave, and in Section 3, we analyzed the photoEMF currents generated by the these light patterns and present some numerical simulations. In Section 4 we report the experiments carried out to verify the theoretical simulations; and in Section 5, we present the discussion and conclusions.

2. LIGHT INTENSITY DISTRIBUTION AFTER THE RONCHI GRATING

In this section we briefly reproduce the known properties of the light field amplitude distribution produced by a Ronchi grating. The treatment mostly follows [4] with slightly different notation.

The electric field as a function of the propagation length z (normalized to $z_0 = \pi$) and the transversal coordinate x is given by the equation

$$E(x, z) = 1/2 + \sum_{n=-\infty}^{\infty} \frac{1}{i\pi} \frac{1}{2n+1} \ \exp(i(2n+1)^2 z + i(2n+1)x). \quad (1)$$

This corresponds to 2π periodic square wave initial conditions:

$$E(x, 0) = 1 \ \text{ if } 0 < x < \pi \ \text{ and } \ E(x, 0) = 0 \ \text{ if } \pi < x < 2\pi. \quad (2)$$

The series in Eq. (1) is quite badly convergent. A simpler expression can be obtained if the propagation length z is set equal to $\pi q/p$ with integers q, p ($z_0 = \pi$). In this case the electric field of the wave as a function of x is a piecewise constant (step) function with discontinuities in points $x = x_m = \pi m/p$ with m being an integer number (Fig. 1). The amplitude of the discontinuity for the electric field in $x = x_m$ defined as

$$\Delta_m = \lim_{\varepsilon \to 0}[E(x_m + \varepsilon) - E(x_m - \varepsilon)] \quad (3)$$

is given by

$$\Delta_m = \frac{1}{p} \sum_{s=0}^{p-1} \exp(i(2s+1)^2 \pi q/p + i(2s+1)m\pi/p). \quad (4)$$

The derivation of Eq. (4) is discussed in detail in [4]. To calculate the total electric field, it is sufficient to perform additions of terms with different m in Eq. (4), taking into account that, due to the symmetry of the Ronchi grating, for $m = 0$, $\mathrm{Re}(E_{+0}) = 1/2 + \mathrm{Re}(\Delta_0/2)$ and $\mathrm{Im}(E_{+0}) = \mathrm{Im}(\Delta_0/2)$, where E_{+0} is the field amplitude for infinitely small positive x. The result of Eq. (4) can be estimated explicitly in terms of Gauss sums (see [4]). For practical calculations, Eq. (4) is easier to compute than employing the Gauss sums, and the calculation is sufficiently fast at least for p of an order of 1000. The direct computation with Eq. (1) is not practical because of its very slow convergence.

From the analysis carried out in [4], it follows that the fractional images of the Ronchi grating with small p values ($p = 2, 3, 4 \ldots$) are relatively simple stepwise functions. However, even very small z displacements from these fractional images produce a transversal structure, which gives a significant contribution to the photoEMF signal. Let us consider a small displacement from the initial distribution at $z = \pi/p$. [The p value is supposed to be large, though Eqs. (5) and (6) below are valid for all p]. By manipulating the Gauss sums, for odd p we obtain

$$\Delta_m = \frac{1}{\sqrt{p}} \ \exp\left(i\frac{\pi}{4}\left[5 - \frac{(p-m)^2}{p}\right]\right) \quad (5)$$

if m is even and

$$\Delta_m = \frac{1}{\sqrt{p}} \ \exp\left(i\frac{\pi}{4}\left[1 - \frac{m^2}{p}\right]\right) \quad (6)$$

if m is odd.

For large p, as a function of the quasi-continuous coordinate $x = \pi m/p$, the derivative of the field using Eq. (6) for x close to $x = 0$ is approximately given by

$$\frac{dE(x)}{dx} \approx \frac{\sqrt{p}}{2\pi} \ \exp\left(i\frac{\pi}{4}[1 - px^2/\pi^2]\right). \quad (7)$$

The contribution of the terms expressed in Eq. (5) to the field close to $x = 0$ can be neglected for large p because there the function given by Eq. (5) rapidly oscillates—it contains the factor $\exp(im\pi/2)$. A similar expression is obtained for x close to π, ($|p - m| \ll p$) using Eq. (3).

Thus, the electric field distribution in the vicinity of the Ronchi grating is approximately expressed in terms of Fresnel integrals [24] on the normalized variable $x\sqrt{p}$. As a function of displacement z, the amplitude of the spikes in these integrals does not diminish when one approximates to the grating ($1/p \to 0$), but the spike widths are proportional to the square root of the distance to the grating. Physically, the result is quite clear—it means that, close to the Ronchi grating, we observe the diffraction from the edges. It is interesting, however, that simple discrete expressions are possible. Equations
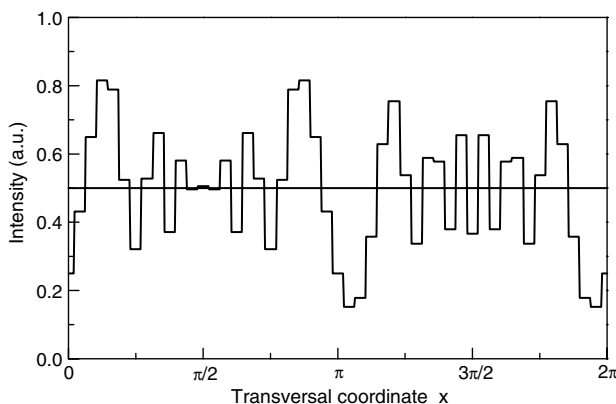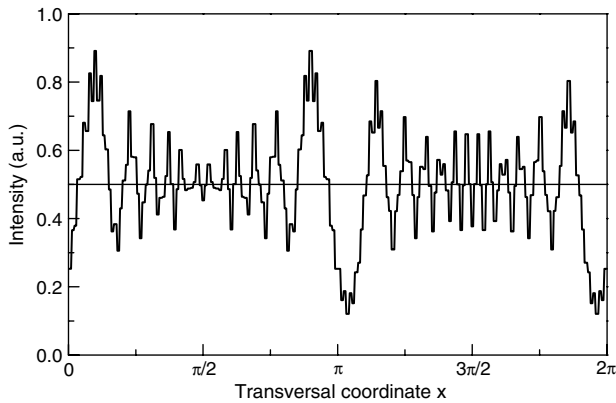
Fig. 1. Theoretical intensity profiles for (a) $z = (\pi/2) - (\pi/390)$ and (b) $z = (\pi/2) - (\pi/96)$. The Talbot distance is normalized to $z_0 = \pi$.

similar to Eqs. (5) and (6) are obtained for even p as well, but they are more complicated, and we do not reproduce them here.

Because of the above-mentioned properties of fractional images, one will observe similar structures near the field discontinuities for all fractional images. In fact, the image at a plane $z = \pi[(q_0/p_0) + (1/p)]$ can be considered as a result of the propagation of the field in a plane $z = \pi(1/p)$ from the position $z' = \pi(q_0/p_0)$. If $p_0 \ll p$, a small number of displaced copies of the distribution at $z = \pi(1/p)$ will be produced, which inherit the structure near the edges. The numerical demonstration of this effect is shown in Fig. 1, close to the characteristic plane $z = \pi/2 = z_0/2$, where the pattern intensity is just constant ($I = |E|^2 = 1/2$), but the electric field itself has a discontinuity in phase. In Fig. 2 a similar effect is depicted for a vicinity of the $z = \pi/3$ plane.

3. PHOTOEMF PRODUCED BY A VIBRATING RONCHI GRATING

The experimental setup for measuring the non-steady-state photoEMF produced by the diffraction of vibrating Ronchi grating is depicted in Fig. 3.

For an intensity distribution $I(x)$ the amplitude of the photoEMF current for vibration amplitude of the illuminating pattern δ at a distance z is approximately given by [9,12]

$$J(\delta, z) \approx J_0 \delta \int_{-\pi}^{\pi} \left(\frac{\partial I(z, x)}{\partial x} \right)^2 \mathrm{d}x. \qquad (8)$$

The characteristic current J_0 is proportional to the average sample photoconductivity [10], which is assumed to be independent of z. For Eq. (8) to be valid, several conditions are necessary: both the vibration amplitude and the crystal diffusion length have to be smaller than a characteristic peak width and the period of the Ronchi grating, the vibration frequency has to be higher than the crystal cutoff frequency, and the contrast of the pattern has to be small (additional illumination is generally required).

For stepwise intensity distributions, such as those obtained for fractional images, Eq. (8) is not valid; instead the characteristic signal for these positions is given by

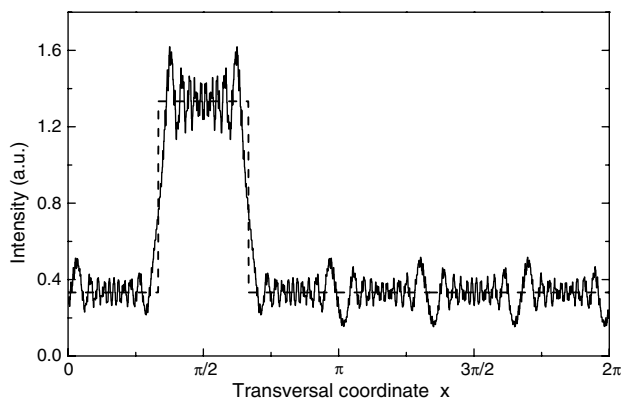$$J(\delta) \approx J_0 \sum_m (\Delta I_m)^2, \qquad (9)$$

Fig. 2. Theoretical intensity distribution for $z = \pi/3$ (square wave) and $z = (160/481)\pi$. The Talbot distance is normalized to $z_0 = \pi$.
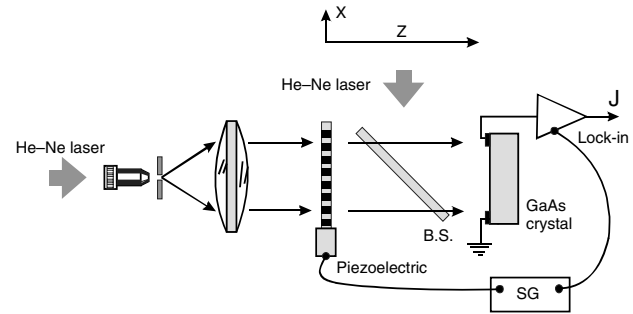

Fig. 3. Experimental setup for measuring the photoEMF currents generated in a GaAs crystal by the diffraction of a vibrating Ronchi grating. SG, signal generator; B.S., beam splitter.

where the sum is taken over all the discontinuities within a period and ΔI_m is the light intensity at each discontinuity step. The vibration amplitude is assumed to be smaller than the distance between the closest discontinuities.

The results according to Eq. (9) of the photoEMF current for fractional images at planes $z_q = \pi q/p$ for p values up to $\sim$100 are given in Fig. 4. All odd values of p produce the same of photocurrent ($J = 2$), just as the one obtained for the initial field at $z = 0$. For $z = \pi/2 = z_0/2$, the current is zero, which corresponds to the position of zero contrast (i.e., a phase grating), and, consequently, there is no photoEMF effect. The second-lowest value of photoEMF is obtained at $z = \pi/4 = z_0/4$. The idealized function presented in Fig. 4 has discontinuities for all rational z/z_0.

For small displacements from simple fractional images, however, Eq. (8) has to be used for finite vibration amplitude. This makes dependences even more complicated because formally the integrals of Eq. (8) diverge for $p \to \infty$, i.e., for all z/π values given by irrational numbers. Thus, practically, one can expect that the dependence of photoEMF on z is a highly complicated multispike function.

To estimate the influence of the finite spatial bandwidth on the z dependence of the photoEMF, we have performed the numerical simulation for the propagation of a $1 + 1D$ Gaussian beam with amplitude $E(x, z)$ that has an initial distribution given by $E(x, z = 0) = \exp(-(x/100)^2)$ modulated by a Ronchi grating with a 2π period. The beam profile upon
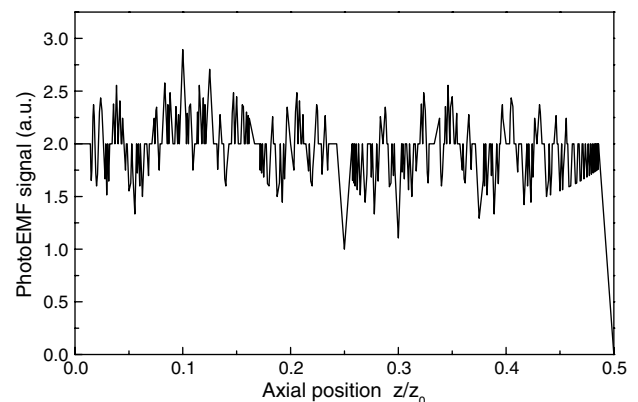

Fig. 4. PhotoEMF calculation for a number of discrete values $z_{q,p} = \pi q/p$. Note that the only plane where the current is zero is $z = \pi/2$ (the last point to the right). The function is highly irregular. The continuous curve is only a guide to the eye for connecting discrete points. The Talbot distance is normalized to $z_0 = \pi$.

propagation was calculated with a fast Fourier transform, and the integral in Eq. (8) was evaluated numerically over 10 central fringes of the image. The grating vibration, some possible misalignments, and the spatial-frequency transfer function of the crystal introduce certain spatial-frequency cutoffs. Taking into account these factors exactly is rather complicated; thus, to study the qualitative influence, we simply abruptly limited the upper Fourier spatial frequency in the x direction by a certain number k_0. The simulation results are shown in Fig. 5 for three different cutoff spatial frequencies. In this plot, we have taken a distance to the grating in a range corresponding to our experimental conditions.

It is observed that the signal approximately conserves a symmetry with respect to planes $z/z_0 = 0.5$ and 1, but generally the degree of this symmetry diminishes when the distance to the grating becomes larger. The principal minimum for $z/z_0 = 0.5$ is distinguished in all three curves as well as a few minima corresponding to fractional images. The amplitude in the principal minimum is not zero. The width of this peak diminishes for larger spatial-frequency bands. The positions of secondary maxima/minima points, however, can vary, depending on the detection band. At the plane $z = z_0$ a local maximum is present, but it is not very pronounced with respect to nearby spikes. For the curve with $k_0 = 15$, it is clearly observed that the high-frequency detail becomes more prominent when one moves closer to the grating.

4. EXPERIMENT

To verify the described theory, we carried out the detection of the photoEMF electrical currents generated by a vibrating Ronchi grating. The setup is depicted in Fig. 3. A 10 mW He–Ne laser beam ($\lambda = 632.8$ nm) was filtered and then collimated by a 20 cm focal length lens with 2.5 cm diameter. The collimated beam illuminated a Ronchi grating of 50 lines/in. (period $d = 0.508$ mm), so the Talbot distance was $z_0 = 407.8$ mm. The vibrations in the grating were induced by attaching it to a low-frequency piezoelectric transducer driven by a signal generator. The amplitude of the induced vibrations was 3 μm at a frequency of 600 Hz. The

GaAs crystal was similar to the one reported in [15]; it had the frontal dimensions of 8 mm × 5 mm and 0.5 mm thick. Two electrodes were deposited with silver paint on the front surface in such a way that the interelectrode area was $L_x = 5$ mm and $L_y = 5$ mm. The diffusion length for this crystal is ≈40 μm. Note that both the amplitude of vibration and the diffusion length of the crystal photocarriers are much smaller than the period of the grating and any characteristic peak width. The current was measured by the voltage drop across the lock-in input impedance, with a integration time of 300 ms. The z axis scan was carried out either by placing the crystal on an optical rail (1 mm steps) or on a linear translational stage with a 10 μm resolution. A uniform background intensity was provided by a second He–Ne laser. The reported experiments were carried out under regular illumination conditions in the laboratory; no special care was taken to block the stray light impinging on the crystal.

Figure 6 shows the photoEMF current generated in the GaAs crystal as a function of the axial distance z in steps of 1 mm.

The positions where the minimum contrast (i.e., minimum photoEMF current) occurs are clearly observed in this dependence; they correspond to the planes $z = z_0/2$ and $z = 3z_0/2$. From the difference between these points, we obtain the value $z_0 = (408 \pm 1)$ mm, which is in very good agreement with the expected theoretical value (407.8 mm). Half-way between these positions, there is a relative maximum that coincides with the first negative Talbot image (i.e., the image of the grating laterally shifted by a half-period.) The letters a, b, and c indicate some spikes of minimum photoEMF current corresponding to fractional distances.

To demonstrate the high spatial resolution of the proposed technique under these conditions, in the Fig. 7 we have plotted the photoEMF current near the first plane of minimum contrast (i.e., in the plane $z = z_0/2$). Figure 7(a) was taken with steps of 0.5 mm and Fig. 7(b) with steps of 100 μm. The fluctuations in the signal are indicated by the error bars, but the uncertainty in the axial position z (± 5 μm) in Fig. 7(b) cannot be plotted in this scale. In Fig. 7(a) note the symmetry around the minimum and that higher spatial-frequency components can be observed at this axial scale in comparison with Fig. 6.
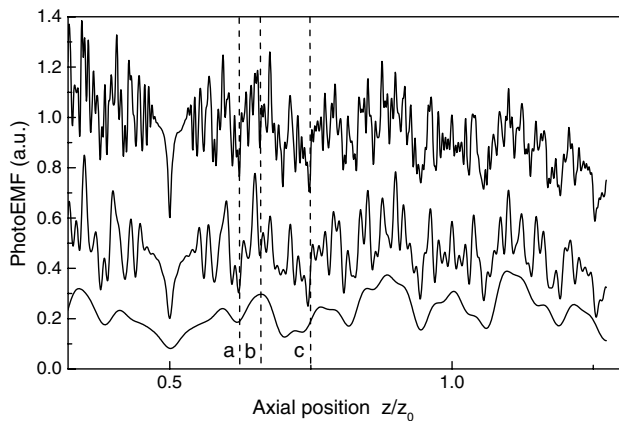

Fig. 5. Computer simulation of the photoEMF signal generated by a vibrating Ronchi grating illuminated by a wide Gaussian beam. The first (negative) self-image is at $z = z_0$; the zero contrast point is $z/z_0 = 0.5$. The detector spatial cutoff frequency is (from the lower to the upper curve) $k_0 = 5, 10, 15$. The $k_0 = 10$ and 15 curves are upward shifted for better visibility. Positions marked as a, b, and c in the $k_0 = 15$ curve correspond to fractional distances 5/8, 2/3, and 3/4 of z_0, respectively.
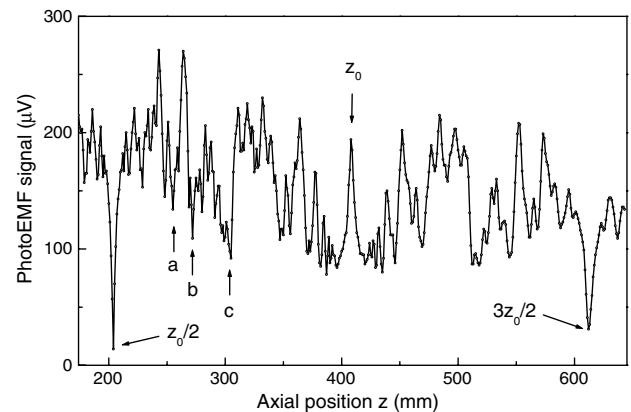

Fig. 6. Experimental photoEMF current generated in a GaAs crystal by a vibrating Ronchi grating as a function of the axial distance from the grating in 1 mm steps. Positions marked a, b, and c correspond to fractional distances 5/8, 2/3, and 3/4 of z_0, respectively.
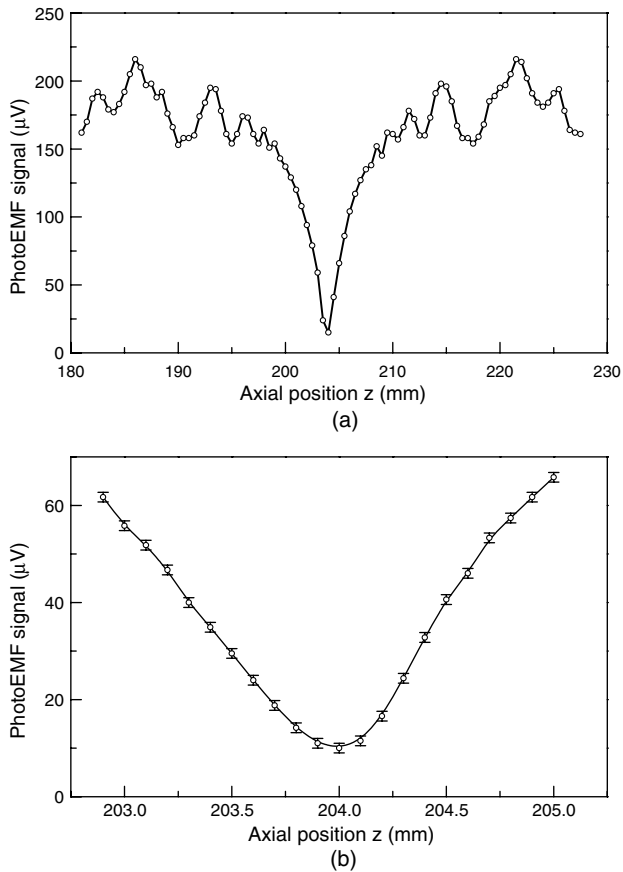
Fig. 7.   PhotoEMF current as a function of the axial position around the first position of minimum contrast at two scanning steps: (a) steps of 0.5 mm and (b) 100 μm. The data were taken with 1 s time constant.

5. DISCUSSION AND CONCLUSIONS

Both theoretical (Fig. 5) and experimental dependences (Fig. 6) show similar behavior: they present a multispike dependence on the propagation distance z, and the positions of minimal (nominally zero) contrast, corresponding to the points of low current, are very well defined. As predicted by the theory, the experimental width of these spikes increases with the propagation distance as well as the signal amplitude in a minimum. The position where the first negative Talbot image occurs ($z = z_0$) is characterized by a relative maximum in the photoEMF signal; however, the height of this spike is not as large as for the spikes around it. As expected, there is an approximate symmetry with respect to this plane, but there are more high-frequency details for distances closer to the Ronchi grating.

Some of the minima are related to fractional images. In particular, in Fig. 6 we have indicated the fractional distances 5/8, 2/3, and 3/4 of z_0. Note that, as predicted by the theory, plane c, with the second lowest value of photoEMF, is the half-way plane between $z_0/2$ and z_0.

From Fig. 7(b) we can estimate the spatial resolution of the photoEMF technique. In the region of minimum contrast we can easily distinguish between positions separated by 100 μm.

In conclusion, the reported experiment represents an interesting manifestation of the fractal structure in the Talbot effect. More complex deterministic structures are observed when the detection spatial-frequency bandwidth becomes

larger. The nature of the detection, sensitive to the intensity derivative, makes these structures especially pronounced in comparison with direct intensity measurements, and the averaging inherent in the photoEMF effect yields high-quality and well-reproducible curves not affected by speckle.

The narrow minima are obtained for some characteristic fractional images. The minima for the planes $z = z_0/2$ and $z = 3z_0/2$ are especially pronounced and easily identified, and its small width permits the determination of Talbot distance with an exactitude of about $z_0/10^4$; this figure is much better than for traditional methods [25,26] based on the averaged pattern contrast, and it can be further improved by optimizing the experimental geometry (in particular by using wider beams) and by diminishing the detector diffusion length. The high accuracy obtained can be useful for optical testing, spectrometry [27], and metrology.

ACKNOWLEDGMENTS

REFERENCES

1. H. F. Talbot, "Facts relating to optical science. No. IV," Philos. Mag. **9**, 401–407 (1836).
2. Lord Rayleigh, "On copying diffraction gratings, and on some phenomena connected therewith," Philos. Mag. **11**, 196–201 (1881).
3. K. Patorsky, "The self-imaging phenomenon and its applications," in Vol. **27** of *Progress in Optics*, E. Wolf, ed., (North Holland, 1989), pp. 1–108.
4. M. V. Berry and S. Klein, "Integer, fractional and fractal Talbot effects," J. Mod. Opt. **43**, 2139–2164 (1996).
5. W. B. Case, M. T. Tomandl, S. Deachapunya, and M. Arndt, "Realization of optical carpets in the Talbot and Talbot–Lau configurations," Opt. Express **17**, 20966–20974 (2009).
6. M. J. J. Vrakking, D. M. Villeneuve, and A. Stolow, "Observation of fractional revivals of a molecular wavepackets," Phys. Rev. A **54**, R3740 (1996).
7. J. A. Yeazell and C. R. Stroud, Jr., "Observation of fractional revivals in the evolution of a Rydberg atomic wave packet," Phys. Rev A **43**, 5153–5156 (1991).
8. M. P. Petrov, I. A. Sokolov, S. I. Stepanov, and G. S. Trofimov, "Non-steady-state photo-electromotive force induced by dynamic gratings in partially compensated photoconductors," J. Appl. Phys. **68**, 2216–2225 (1990).
9. S. Stepanov, "Photo-electromotive force in semiconductors," In *Handbook of Advanced Electronic and Photonic Materials and Devices*, H. S. Nalwa, ed., (Academic, 2001), Vol. **2**, pp. 205–272.
10. S. Stepanov, P. Rodriguez, S. Mansurova, M. L. Arroyo, S. Trivedi, and C. C. Wang, "Wavelength dependence of the photo-electromotive-force effect in CdTe:V crystal with bipolar photoconductivity," Opt. Mater. **29**, 623–630 (2007).
11. S. Stepanov, P. Rodriguez, S. Trivedi, and C. C. Wang, "Effective broadband detection of nanometer laser-induced ultrasonic surface displacements by CdTe:V adaptive photoelectromotive force detector," Appl. Phys. Lett. **84**, 446–448 (2004).
12. N. Korneev, P. Rodriguez, and S. Stepanov, "2D pattern matching with adaptive photodetectors," Opt. Commun. **134**, 514–520 (1997).
13. Y. Ding, I. Lahiri, D. Nolte, G. J. Dunning, and D. M. Pepper, "Electric-field correlation of femtosecond pulses by use of a photoelectromotive force detector," J. Opt. Soc. Am. B **15**, 2013–2017 (1998).
14. M. L. Arroyo-Carrasco, P. Rodriguez-Montero, and S. Stepanov, "Measurement of the coherence length of diffusely scattered laser beams with adaptive photodetectors," Opt. Commun. **157**, 105–110 (1998).

15. P. Rodríguez-Montero, C. M. Gómez-Sarabia, and J. Ojeda-Castañeda, "Adaptive photodetector for assisted Talbot effect," Appl. Opt. **47**, 3778–3783 (2008).
16. A. W. Lohmann and D. Silva, "An interferometer based on the Talbot effect," Opt. Commun. **2**, 413–415 (1971).
17. Y. Nakano and K. Murata, "Talbot interferometry for measuring the focal length of a lens," Appl. Opt. **24**, 3162–3166 (1985).
18. M. P. Kothiyal and R. S. Sirohi, "Improved collimation testing using Talbot interferometry," Appl. Opt. **26**, 4056–4057 (1987).
19. M. Tebaldi, G. Forte, R. Torroba, N. Bolognini, and A. Tagliaferri, "Self-imaging pitch variation applied to focal length digital measurements," Opt. Commun. **250**, 10–15 (2005).
20. P. Chavel and T. C. Strand, "Range measurement using Talbot diffraction imaging of gratings," Appl. Opt. **23**, 862–871 (1984).
21. G. Schirripa Spagnolo, D. Ambrosini, and D. Paoleti, "Displacement measurement using the Talbot effect with a Ronchi grating," J. Opt. A. **4**, S376–S380 (2002).
22. S. Prakash, S. Upadhyay, and C. Shakher, "Real time out-of-plane vibration measurement/monitoring using Talbot interferometry," Opt. Lasers Eng. **34**, 251–259 (2000).
23. C.-F. Kao and M.-H. Lu, "Optical encoder based on the fractional Talbot effect," Opt. Commun. **250**, 16–23 (2005).
24. W. Gautschi, *Handbook of Mathematical Functions with Formulas, Graphs, and Mathematical Tables*, M. Abramowitz and I. A. Stegun, eds., (National Bureau of Standards, 1972), Chap. 7.3.
25. R. Torroba, N. Bolognini, M. Tebaldi, and A. Tagliaferri, "Positioning method based on digital Moiré," Opt. Commun. **209**, 1–6 (2002).
26. M. Takeda, H. Ina, and S. Kobayashi, "Fourier-transform method of fringe-pattern analysis for computer-based topography and interferometry," J. Opt. Soc. Am. **72**, 156–160 (1982).
27. H. L. Kung, A. Bhatnagar, and D. A. B. Miller, "Transform spectrometer based on measuring the periodicity of Talbot self-images," Opt. Lett. **26**, 1645–1647 (2001).